FSU-HEP-951030
ITP-SB-95-15
LBL-37266

Reanalysis of the EMC charm production data with extrinsic and intrinsic charm at NLO

B. W. Harris
Physics Department,
Florida State University,
Tallahassee, Florida 32306-3016 USA

J. Smith
Institute for Theoretical Physics,
State University of New York at Stony Brook,
Stony Brook, New York 11794-3840 USA

and

R. Vogt[1]
Nuclear Science Division,
Lawrence Berkeley Laboratory,
Berkeley, California 94720 USA
and
Physics Department,
University of California at Davis,
Davis, California 95616 USA

November 1995

Abstract

A calculation of the next-to-leading order exclusive extrinsic charm quark differential distributions in deeply inelastic electroproduction has recently been completed. Using these results we compare the NLO extrinsic contributions to the charm structure function $F_2(x, Q^2, m_c^2)$ with the corresponding

[1]This work was supported in part by the Director, Office of Energy Research, Division of Nuclear Physics of the Office of High Energy and Nuclear Physics of the U. S. Department of Energy under Contract Number DE-AC03-76SF0098.

NLO intrinsic contributions. The results of this analysis are compared with the EMC DIS charm quark data and evidence for an intrinsic charm component in the proton is found.

1 Introduction

The European Muon Collaboration (EMC) [1] has played an important role in the study of charmed quark production in deep inelastic scattering. Their results established that photon-gluon fusion in QCD, the analogue of the Bethe-Heitler reaction in QED, explains most of the charmed quark contribution to the deep inelastic structure function F_2. The scattering cross section for the reaction $e^-(l_1) + P(p) \to e^-(l_2) + c(p_1) + X$ is conventionally written as a differential in x and y as

$$\frac{d^2\sigma}{dxdy} = \frac{2\pi\alpha^2}{Q^4} S \left[\left\{ 1 + (1-y)^2 \right\} F_2(x, Q^2, m_c^2) - y^2 F_L(x, Q^2, m_c^2) \right] \quad (1.1)$$

with $q = l_1 - l_2, Q^2 = -q^2, x = Q^2/2p \cdot q$ and $y = p \cdot q / p \cdot l_1$. The dependence on the charm quark mass, m_c, is shown explicitly. The square of the center-of-mass energy of the electron-proton system is S. The above formula holds after integration over the azimuthal angle between the plane containing the incoming and outgoing electron and the plane containing the incoming proton and outgoing charmed quark. In a typical experimental extraction of F_2 from σ, the F_L contribution is either neglected or approximated by leading order QCD.

The lowest order (LO) photon-gluon fusion model in QCD is based on the twist-two term in the operator product expansion which incorporates the factorization theorem [2] for hard scattering. The EMC $F_2(x, Q^2, m_c^2)$ data was not in complete agreement with the predictions of this model at all x and Q^2. The disagreement at large x and Q^2 substantiated the claim that a second (higher twist) component of charm production was necessary, called intrinsic charm (IC) [3] to distinguish it from the twist-two mechanism, referred to as extrinsic charm (EC).

In the analysis of the EMC data [1], a relatively simple model was used for both the EC and IC components. At the time, only the LO contributions to $F_2(x, Q^2, m_c^2)$ from both models were available. Afterwards, Hoffman and Moore [4] calculated the next-to-leading order (NLO) corrections to the IC component and discussed their effects on the EMC analysis. Based on LO photon-gluon fusion, they found evidence for an 0.3 % IC component in the proton. Due to the lack of NLO calculations of the EC component for the analysis of the EMC data, the previous results are inconclusive.

The NLO corrections to the extrinsic component are now also available [5, 6, 7, 8, 9]. These NLO calculations yield large cross sections in specific regions of phase space since new mechanisms occur, such as the t-channel exchange of massless gluons. Hence cross sections for "massive" quark production in NLO should really not be compared with the LO prediction via the standard K factor, although this is often done in the literature. We will comment on this later.

The single particle inclusive results [7] for the charmed quark distributions were applied to the EMC data in [10] without addressing the IC component. However, even the single particle inclusive NLO results are not enough for a complete reanalysis of the EMC data since the invariant mass of the $c\overline{c}$ pair, $M_{c\overline{c}}$, was included in the scale of the running coupling constant and cuts were made on the energies of the decay muons. Thus an exclusive NLO calculation, retaining all possible information on both the charmed and the anticharmed quarks, is required. The NLO corrections to exclusive production were derived in [8, 9], making it possible to include $M_{c\bar{c}}$ in the running coupling constant. Since the complete NLO results are now available for both EC and IC production, a more detailed QCD analysis of the EMC results is finally possible, allowing us to make a more reliable determination of the IC content of the proton.

To make this paper self-contained, we begin with a review of intrinsic charm and its NLO contribution to the structure function $F_2(x, Q^2, m_c^2)$ in Section 2. We follow this with a brief review of extrinsic charm and its NLO contribution to $F_2(x, Q^2, m_c^2)$ in Section 3. In Section 4 we discuss the results of our analysis and conclude that, even with the addition of the new NLO EC contributions and the use of the most recent parton densities, an IC component is still needed to fit the EMC data.

2 The Intrinsic Charm Component

The QCD wavefunction of a hadron can be represented as a superposition of quark and gluon Fock states. For example, at fixed light-cone time, $\tau = t + z/c$, the proton wavefunction can be expanded as a sum over the complete basis of free quark and gluon states: $|\Psi_p\rangle = \sum_m |m\rangle \, \psi_{m/p}(x_i, k_{T,i}, \lambda_i)$ where the color-singlet states, $|m\rangle$, represent the fluctuations in the proton wavefunction with the Fock components $|uud\rangle$, $|uudg\rangle$, $|uudc\overline{c}\rangle$, *etc.* The

boost-invariant light-cone wavefunctions, $\psi_{m/p}(x_i, k_{T,i}, \lambda_i)$, needed to compute probability distributions, are functions of the relative momentum coordinates $x_i = k_i^+/P^+$ and $k_{T,i}$. Momentum conservation demands $\sum_{i=1}^n x_i = 1$ and $\sum_{i=1}^n \vec{k}_{T,i} = 0$, where n is the number of partons in a Fock state $|m\rangle$. When an interaction occurs, the coherence of the Fock components is broken and the fluctuations can hadronize, forming new hadronic systems [11]. For example, intrinsic $c\overline{c}$ fluctuations [3] can be liberated provided the system is probed during the characteristic time, $\Delta t = 2p_{\rm lab}/M^2_{c\overline{c}}$, that such fluctuations exist.

There is substantial circumstantial evidence for the existence of intrinsic $c\overline{c}$ states. Leading charm production in πN [12] and hyperon-N [13] collisions requires a charm source beyond leading twist. The leading charm production can be explained by the coalescence of intrinsic charmed quarks in the projectile wavefunction with spectator valence quarks [14, 15]. Final state coalescence mechanisms [16] cannot consistently describe data with meson and baryon projectiles. The NA3 experiment has shown that the single J/ψ cross section at large x_F is greater than expected from gg and $q\overline{q}$ production [17, 18]. This experiment has also measured a significant number of correlated J/ψ pairs [19] which carry a larger fraction of the projectile momentum than expected from leading-twist QCD. Intrinsic heavy quark states such as $|\overline{u}dc\overline{c}c\overline{c}\rangle$ can explain the production of fast J/ψ pairs [20]. Additionally, intrinsic charm may account for the anomalous longitudinal polarization of the J/ψ at large x_F [21] seen in $\pi N \to J/\psi X$ interactions.

Microscopically, the intrinsic heavy quark Fock component in the proton wavefunction, $|uudc\overline{c}\rangle$, is generated by virtual interactions such as $gg \to Q\overline{Q}$ where the gluons couple to two or more valence quarks. The probability for $c\overline{c}$ fluctuations to exist in a light hadron thus scales as $\alpha_s^2(m_c^2)/m_c^2$ relative to leading-twist production [14]. Therefore, this contribution is higher twist, suppressed by $\mathcal{O}(1/m_c^2)$ compared to extrinsic production.

The dominant Fock state configurations are not far off shell and thus have minimal invariant mass, $M^2 = \sum_i m^2_{T,i}/x_i$ where $m_{T,i} = \sqrt{k^2_{T,i} + m_i^2}$ is the transverse mass of parton i in the state. Intrinsic $c\overline{c}$ Fock components with minimum invariant mass correspond to configurations with equal rapidity constituents. Thus, unlike extrinsic heavy quarks generated from a single parton, intrinsic heavy quarks carry a larger fraction of the parent momentum than the light quarks in the state [3]. It was shown that large

x_F virtual $c\overline{c}$ or lepton pairs can be liberated by a relatively soft interaction [11]. For soft interactions at momentum scale μ_s, the intrinsic heavy quark cross section is suppressed by a resolving factor proportional to $\mu_s^2/4m_c^2$ [14] for hadroproduction and $(\mu_s^2+Q^2)/(4m_c^2+Q^2)$ for electroproduction [11, 22].

The general form of the Fock state wavefunction appropriate to any frame at fixed light-cone time is

$$\Psi(\vec{k}_{\perp i}, x_i) = \frac{\Gamma(\vec{k}_{\perp i}, x_i)}{m_h^2 - M^2} \ , \tag{2.1}$$

where Γ is a vertex function, expected to be a decreasing function of $m_h^2 - M^2$, a measure of the "off-shellness" of the Fock state fluctuation. The vertex function is assumed to be relatively slowly varying; the particle distributions are then controlled by the light-cone energy denominator and phase space. This form for the higher Fock components is applicable to an arbitrary number of light and heavy partons. The Fock states containing charmed quarks can be materialized by a soft collision in the target which brings the state on shell. In the limit of zero binding energy, Ψ is singular and the fractional momenta peak at $x_i = m_i/m_h$. Note that the denominator is minimized when the heaviest constituents carry the largest fraction of the longitudinal momentum. The parton distributions reflect the underlying shape of the Fock state wavefunction. Assuming it is sufficient to use a mean value of k_T^2 to calculate the x distributions, the probability distribution for a general n–particle intrinsic $c\overline{c}$ Fock state as a function of x is

$$\frac{dP_{\rm ic}}{dx_i \cdots dx_n} = N_n[\alpha_s^2(M_{c\overline{c}})]^2 \ \frac{\delta(1-\sum_{i=1}^n x_i)}{(m_h^2 - \sum_{i=1}^n (\widehat{m}_i^2/x_i))^2} \ , \tag{2.2}$$

where $\widehat{m}_i = \sqrt{m_i^2 + \langle \vec{k}_{T,i}^2 \rangle}$ is the average transverse mass and N_n normalizes the Fock state probability. In the heavy quark limit, $\widehat{m}_c$, $\widehat{m}_{\overline{c}} \gg m_h$, $\widehat{m}_q$ and the probability reduces to

$$\frac{dP_{\rm ic}}{dx_i \cdots dx_n} = N_n[\alpha_s^2(M_{c\overline{c}})]^2 \frac{x_c^2 x_{\overline{c}}^2}{(x_c + x_{\overline{c}})^2} \ \delta(1 - \sum_{i=1}^n x_i) \ . \tag{2.3}$$

Integration over the light quarks and anticharmed quark momenta for $n = 5$, the minimal intrinsic charm Fock state of the proton, $|uudc\overline{c}\rangle$, gives

the intrinsic charmed quark density distribution as a function of the charmed quark momentum fraction,

$$c(x) \propto \frac{dP_{\rm ic}(x)}{dx} = \frac{1}{2}N_5 x^2[\frac{1}{3}(1-x)(1+10x+x^2) + 2x(1+x)\ln x] \ . \quad (2.4)$$

If there is a 1% probability for intrinsic charm in the nucleon, as previously suggested [3], then $N_5 = 36$. The charmed quark structure function at leading order $F_2^{(0)}(x)$ is given by

$$F_2^{(0)}(x) = 8xc(x)/9 \, , \quad (2.5)$$

in the limit where the charmed quark mass is negligible. In a complete analysis of the EMC charm data, the massless result is clearly inapplicable.

Hoffmann and Moore [4] incorporated mass effects into the above analysis. They first introduced a mass scaling variable $\xi = 2ax[1+(1+4\rho x^2)^{1/2}]^{-1}$ where $\rho = m_p^2/Q^2$, $a = [(1+4\lambda)^{1/2}+1]/2$ and $\lambda = m_c^2/Q^2$. The proton mass is denoted by m_p. The $c\overline{c}$ mass threshold imposes the constraint $\xi \leq \gamma < 1$ where $\gamma = 2a\hat{x}[1+(1+4\rho\hat{x}^2)^{1/2}]^{-1}$. Then (2.5) is replaced by

$$F_2^{(0)}(x, Q^2, m_c^2) = 8\xi c(\xi, \gamma)/9 \, , \quad (2.6)$$

with $c(z,\gamma) = c(z) - zc(\gamma)/\gamma$ for $z \leq \gamma$ and zero otherwise; $c(z)$ is defined in (2.4). Hoffmann and Moore found that further mass effects could be incorporated by generalizing the operator-product expansion analysis to include both the charmed quark and target masses. The final LO result, *c.f.* eq. (18) in [4], is then

$$F_2^{(0)}(x, Q^2, m_c^2) = \frac{8x^2}{9(1+4\rho x^2)^{3/2}} \left[\frac{(1+4\lambda)}{\xi}c(\xi,\gamma) + 3\hat{g}(\xi,\gamma)\right] \, , \quad (2.7)$$

where

$$\hat{g}(\xi,\gamma) = \frac{2\rho x}{(1+4\rho x^2)} \int_\xi^\gamma dt \frac{c(t,\gamma)}{t}\left(1 - \frac{\lambda}{\rho t^2}\right)\left[1 + 2\rho x t + \frac{2\lambda x}{t}\right] \, . \quad (2.8)$$

The NLO IC component of the structure function is given by

$$F_2^{(1)}(x, Q^2, m_c^2) = \frac{8}{9}\xi \int_{\xi/\gamma}^1 \frac{dz}{z} c(\xi/z, \gamma)\sigma_2^{(1)}(z, \lambda) \, . \quad (2.9)$$

When the lowest order cross section is normalized to

$$\sigma_2^{(0)}(z,\lambda) = \delta(1-z), \tag{2.10}$$

the NLO QCD corrections to the IC contribution are given by eq. (51) in [4],

$$\begin{aligned}
\sigma_2^{(1)}(z,\lambda) &= \frac{2\alpha_s}{3\pi}\delta(1-z)\Big\{4\ln\lambda - 2 + \sqrt{1+4\lambda}L + \frac{(1+2\lambda)}{\sqrt{1+4\lambda}}[3L^2 \\
&+ 4L + 4\mathrm{Li}_2(-d/a) + 2L\ln\lambda - 4L\ln(1+4\lambda) + 2\mathrm{Li}_2(d^2/a^2)]\Big\} \\
&+ \frac{\alpha_s}{3\pi}\frac{1}{(1+4\lambda z^2)^2}\Big\{\frac{1}{[1-(1-\lambda)z]^2} \\
&\times[(1-z)(1-2z-6z^2+8z^4) + 6\lambda z(1-z)(3-15z-2z^2+8z^3) \\
&+ 4\lambda^2 z^2(8-77z+65z^2-2z^3) + 16\lambda^3 z^3(1-21z+12z^2) - 128\lambda^4 z^5] \\
&- \frac{2\hat{L}}{\sqrt{1+4\lambda z^2}}[(1+z)(1+2z^2) - 2\lambda z(2-11z-11z^2) - 8\lambda^2 z^2(1-9z)] \\
&- \frac{8z^4(1+4\lambda)^2}{(1-z)_+} - \frac{4z^4(1+2\lambda)(1+4\lambda)^2\hat{L}}{\sqrt{1+4\lambda z^2}(1-z)_+}\Big\},
\end{aligned} \tag{2.11}$$

where

$$\hat{L} = \ln\left[\frac{4\lambda z[1-(1-\lambda)z]}{(1+2\lambda z+\sqrt{1+4\lambda z^2})^2}\right]. \tag{2.12}$$

The leading-logarithmic approximation to this formula, given by eq. (54) in the same paper, is

$$\begin{aligned}
\tilde{\sigma}_2^{(1)}(z,\lambda) &= \frac{\alpha_s}{3\pi}\left\{\frac{(1-2z-6z^2)}{(1-z)_+} - \frac{2(1+z^2)\ln z}{1-z}\right. \\
&\quad - \frac{2(1+z^2)\ln\lambda}{(1-z)_+} - 2(1+z^2)\Big[\frac{\ln(1-z)}{1-z}\Big]_+ \\
&\quad \left.-\delta(1-z)[3\ln\lambda + 5 + 2\pi^2/3]\right\}.
\end{aligned} \tag{2.13}$$

The implementation of the plus distributions in eqs. (2.11) and (2.13) is standard [23] :

$$\int_a^1 dx f(x)\left(\frac{1}{1-x}\right)_+ = \int_a^1 dx\frac{f(x)-f(1)}{1-x} + f(1)\ln(1-a) \tag{2.14}$$

$$\int_a^1 dx f(x) \left(\frac{\ln(1-x)}{1-x} \right)_+ = \int_a^1 dx \frac{f(x)-f(1)}{1-x} \ln(1-x) + \frac{1}{2} f(1) \ln^2(1-a). \quad (2.15)$$

In our calculations of the IC contributions to $F_2(x, Q^2, m_c^2)$ we have assumed a 1% probability for IC in the proton. To compare with the original EMC analysis, we take $m_c = 1.5$ GeV and fix the renormalization scale in the one loop running coupling constant to $\mu^2 = Q^2 + 20\,\mathrm{GeV}^2$ and $\Lambda^{(4)}_{QCD} = 0.5$ GeV. Later, when the EC calculations are updated with more recent parton densities, we take the same value of $\Lambda^{(4)}_{QCD}$ as in the parton densities and use the two loop running coupling constant to be consistent with the EC results.

Figure 1 shows the LO and NLO IC contributions to $F_2(x, Q^2, m_c^2)$ for two Q^2 values, $Q^2 = 7$ and 70 GeV^2. The upper dotted line shows the massless (Q^2 independent) result, (2.5), the dot-dashed line shows the ξ scaling formula, (2.6), and the upper solid line shows the full result, (2.7), all at LO. At low Q^2 there is substantial difference between the simple form given in (2.5) and the kinematically corrected formula in (2.7). The three curves are nearly indistinguishable when Q^2 is large, as seen in Fig. 1(b). In the same figure we also show the NLO corrections calculated using eq. (2.9). These are the leading-logarithmic approximation eq. (2.13), dotted lines, and the complete result, eq. (2.11), dashed lines. These two formulae yield different curves at small Q^2 but are almost identical at large Q^2.

We note here that we have uncovered an error in the implementation of eq. (2.9) in recent work [24]: the constant term in eq. (2.14), $f(1)\ln(1-a)$, was omitted. This term is due to the non-zero lower limit of integration in eq. (2.9) and has a large numerical effect. Contrary to [24], our results show that the heavy quarks evolve faster than the massless quarks using the standard DGLAP equations, as suggested by the original results of Hoffmann and Moore [4].

In the remainder of this paper, for the IC results at NLO, we use the sum of the kinematically corrected LO result, eq. (2.7), and the full NLO correction obtained by using eq. (2.9) with eq. (2.11). The result is given by the lower (at $x = 0.4$) solid line in Fig. 1. Note that this total is actually negative at large x and Q^2, indicating that even higher order terms are needed in the perturbation expansion in this region.

3 The Extrinsic Charm Component

Order α_s QCD corrections to the charmed quark structure functions for inclusive production in deep inelastic scattering were first presented in [5]. Heavy quark production was assumed to be extrinsic so that F_2 and F_L could be calculated from the *inclusive* virtual photon-induced reaction $\gamma^*(q)+P(p) \to c(p_1)+X$. The parton level interaction is

$$\gamma^*(q) + a_1(k_1) \to c(p_1) + \overline{c}(p_2) + a_2(k_2) \tag{3.1}$$

where a_1 and a_2 are massless partons and p_2 and k_2 are integrated over in the inclusive calculation. The structure functions can then be written as

$$\begin{aligned} F_k(x,Q^2,m_c^2) &= \frac{Q^2\alpha_s(\mu^2)}{4\pi^2 m_c^2}\int_{\xi_{\min}}^1 \frac{d\xi}{\xi}\left[\, e_c^2 f_{g/P}(\xi,\mu^2) c_{k,g}^{(0)}\,\right] \\ &+ \frac{Q^2\alpha_s^2(\mu^2)}{\pi m_c^2}\int_{\xi_{\min}}^1 \frac{d\xi}{\xi}\left\{ e_c^2 f_{g/P}(\xi,\mu_c^2)\left(c_{k,g}^{(1)} + \overline{c}_{k,g}^{(1)}\ln\frac{\mu^2}{m_c^2}\right)\right. \\ &+ \sum_{i=q,\overline{q}} f_{i/P}(\xi,\mu^2)\left[e_c^2\left(c_{k,i}^{(1)} + \overline{c}_{k,i}^{(1)}\ln\frac{\mu^2}{m_c^2}\right)\right. \\ &+ \left.\left. e_i^2\, d_{k,i}^{(1)} + e_c\, e_i\, o_{k,i}^{(1)}\,\right]\right\}\,, \end{aligned} \tag{3.2}$$

where $k = 2, L$. The lower boundary on the integration is $\xi_{\min} = x(4m_c^2 + Q^2)/Q^2$. The parton momentum distributions in the proton are denoted by $f_{i/P}(\xi,\mu^2)$ where μ, the mass factorization scale, has been set equal to the renormalization scale in the running coupling constant α_s. Finally, $c_{k,i}^{(l)}$ and $\overline{c}_{k,i}^{(1)}\,, (l=0,1)$, and $d_{k,i}^{(1)}$ and $o_{k,i}^{(1)}$ are scale independent parton coefficient functions. In eq. (3.2) the coefficient functions are distinguished by their origin: $c_{k,i}^{(l)}$ and $\overline{c}_{k,i}^{(1)}$ originate from the virtual photon-charmed quark coupling and therefore appear for both charged and neutral parton-induced reactions; $d_{k,i}^{(1)}$ arise from the virtual photon-light quark coupling; $o_{k,i}^{(1)}$ come from the interference between these processes. All charges are in units of e. We have included the terms proportional to $e_c e_i$ in (3.2) even though they do not contribute to the total partonic cross section. We have also isolated the mass factorization scale dependent terms, proportional to $\overline{c}_{k,i}^{(1)}$. Finally, note that eq. (3.2) only holds for $Q^2 > 0$. In the photoproduction limit there are additional terms involving the parton densities in the photon [25, 26, 27, 28].

Recently, two of us have reported on the results of a calculation of the NLO corrections for heavy quark *exclusive* distributions at fixed x and Q^2 [8, 9]. This allows us to study correlations between the outgoing particles in eq. (3.1). The exclusive results are needed for our reanalysis of the EMC data because in the original analysis [1], the strong coupling constant was evaluated at the scale $\mu^2 = Q^2 + M^2_{c\overline{c}}$. Contrary to what was assumed in previous analysis of the IC component, $M_{c\overline{c}}$ is not a constant but a function of x and Q^2 [9].

Since the NLO calculations were not available at the time of the EMC experiment, it is clearly interesting to make a reanalysis of their data including both the NLO corrections and more recent parton densities. For a complete description at NLO, we have included the quark and antiquark contributions to charm production as well as the gluon contribution. See [8] for details.

Our analysis is done in two steps. We begin with the same parameters as used in the EMC analysis [1] to confirm that we can reproduce their EC results at LO. Using these same parameters, we then calculate the NLO contribution to see what effect it would have had. We have used $m_c = 1.5$ GeV/c^2 and the one loop running coupling constant at scale $\mu^2 = Q^2 + M^2_{c\overline{c}}$ with $\Lambda^{(4)}_{QCD} = 0.5$ GeV. In conjunction with the one loop coupling, the scale independent gluon density $xg(x) = 3(1-x)^5$ was also used. We will see that the EC NLO calculation yields values of $F_2(x, Q^2, m_c^2)$ which are above the data. This can be corrected by adjusting the normalization of the theoretical prediction.

Next we repeat the analysis with modern parton distributions and the two loop running coupling constant evaluated at $\mu^2 = Q^2 + M^2_{c\overline{c}}$. The CTEQ3 $\overline{\rm MS}$ parton distributions with $\Lambda^{(4)}_{QCD} = 0.239$ GeV [29] are used. We also compare with MRS [30] and the most recent GRV [31] parton distributions to investigate the dependence on the parton densities.

4 Results

We first show the IC and EC results for $F_2(x, Q^2, m_c^2)$ as a function of Q^2 for fixed ν and study the differences between the NLO and LO results with the running coupling scale and gluon distribution used by EMC [1]. We retrieved $F_2(x, Q^2, m_c^2)$ in bins of x and Q^2 from the Durham-RAL HEP Database [32]. The central x and Q^2 values, $\overline{x}$ and $\overline{Q^2}$, give the average value of ν,

$\overline{\nu} = \overline{Q^2}/2m_p\overline{x}$. The results corresponding to the three curves in Fig. 13 of the EMC paper are presented in Fig. 2 for $\overline{\nu} = 168$, 95, and 53 GeV. Note that the ν bin widths quoted in [1] are $160 < \nu < 220$, $100 < \nu < 160$, and $60 < \nu < 100$, all in GeV. At the values of Q^2 relevant to the EMC data, the mass of the charmed quark is not negligible. Thus the charmed quark cannot be treated as massless and absorbed in the parton densities.

Figure 2 shows the EMC data with our calculations of the LO EC contribution (dotted lines), the NLO EC contribution (solid lines), the LO IC contribution (dot-dashed lines), and NLO IC contribution (dashed lines). The LO EC contribution agrees with the EMC result, as expected, since we used their gluon density. Clearly the EC component can be reduced to improve the agreement of the NLO results with the EMC data by changing the normalization of the gluon density. This also requires some readjustment in the normalization of the charged parton densities to maintain the momentum sum rule. In any case, the data cannot be reconciled with the EC prediction alone since such a readjustment will not fit the data at large $\overline{\nu}$ and Q^2.

We next show the EMC data for the structure function $F_2(x, Q^2, m_c^2)$ at $\bar{\nu} = 53$ GeV in Fig. 3(a) plotted as a function of x. Also in the same figure we add the theory predictions for the LO EC contribution, the NLO EC contribution, the LO IC contribution and the NLO IC contribution. Again we have used the EMC gluon density so that the LO EC result fits most of the data at small x while the IC component is important at larger x. Figures 3(b) and 3(c) show the corresponding results for $\bar{\nu} = 95$ GeV and 168 GeV respectively. It is again true that if we readjust the normalization of the gluon density to move the theory curves down we still cannot get a good fit to the data using only the EC NLO result.

Rather than elaborate on refitting the old EMC gluon density, we turn to a comparison of modern gluon densities with the data. In Fig. 4 we again show $F_2(x, Q^2, m_c^2)$ for fixed $\bar{\nu}$ versus x with the corresponding theoretical curves for the CTEQ3 parton densities [29] obtained from global fits to deep-inelastic, Drell-Yan and direct photon production data. Note that the EMC data have not been used in the global analysis to obtain the parton densities. For consistency $m_c = 1.5$ GeV/c^2 was used in both the EC and IC contributions. The two-loop α_s with $\Lambda^{(4)}_{\rm QCD} = 0.239$ GeV and matching across mass thresholds was used for the EC results which are shown for scales $\mu = \mu_0/2, \mu = \mu_0$ and $\mu = 2\mu_0$ where $\mu_0^2 = Q^2 + M_{c\bar{c}}^2$. We also show

the NLO EC component calculated at $\mu = \mu_0$ using the MRS(G) [30] parton densities with $\Lambda^{(4)}_{\rm QCD} = 0.255$ GeV and the GRV [31] parton densities with $\Lambda^{(4)}_{\rm QCD} = 0.200$ GeV. All parton densities give essentially the same results as there is very little difference between the parton densities in this x and Q^2 range. To demonstrate this we present average values of x in the $\bar{\nu}$ bins for all the parton density and scale combinations in Table 1. Finally the IC component is shown using the two loop $\alpha_s(\mu)$ and the values of $\Lambda_{\rm QCD}$ determined by the parton densities. It is clear that the data cannot be fit with only the EC contribution, even with the most recent parton densities.

We now discuss this conclusion in more detail. To fit the data at NLO a considerable enhancement in $F_2(x, Q^2, m_c^2)$ is needed at large x, significantly beyond that shown in Fig. 4. The K factor, $F_2^{NLO}(x, Q^2, m_c^2)/F_2^{LO}(x, Q^2, m_c^2)$, would then have to have a strong x dependence. To illustrate the variations between the LO and NLO EC results the K factors, calculated with NLO parton densities in the numerator and denominator and with the two-loop α_s, are shown in Fig. 5 as functions of x for the EMC $\bar{\nu}$ values. We have also computed the K factors with the LO parton densties (available for CTEQ3 and GRV) and the lowest order coefficient functions with the one-loop α_s in the denominator and the NLO parton densities with the two-loop α_s in the numerator, as advocated in [10]. Although some differences in the K factors are observable, they are not large enough to affect our conclusions. We want to remind the reader that the NLO corrections to heavy quark production contain dynamical mechanisms which lead to large enhancements in the cross sections [25, 33, 34] at NLO. An analogous situation in QED would be a comparison of the muon pair production cross section in the reaction $e^+e^- \to \mu^+\mu^-$ in LO, where there is an s-channel pole, with the NLO muon pair production by the two photon mechanism, $e^+e^- \to e^+e^-\mu^+\mu^-$, which has a t-channel pole. At large energies, the two photon mechanism clearly yields a larger cross section but this does not violate the convergence of the perturbative expansion for QED. Therefore it is unwise to place too much emphasis on a comparison with the LO results.

The increase in the K factor appears at large Q^2 and large x, close to threshold, as may be expected [7]. However, the most important issue is whether or not the K factor is a constant in the region of the EMC data. A constant K factor would lead to a uniform enhancement of the EC component without improving the fit at large x. Indeed, the K factors change by 10-

30% for the higher $\bar{\nu}$ bins at large x, not enough to significantly affect the results. In the lowest $\bar{\nu}$ bin, the K factor increases by nearly a factor of two, but the EC results are steeply falling and are negligible compared to the IC contribution for $x > 0.3$. Therefore, in the x region covered by EMC, we see that the K factor does not change enough to affect our conclusions regarding the need for an IC component.

In Fig. 6 we show the corresponding K factors for the IC component. The opposite behavior to the EC component is observed–the K factor falls with x, flattening at large x. This is also clearly a threshold effect since the largest K factors appear at the highest $\bar{\nu}$ and lowest x. In this region, close to threshold, the IC component is negligible compared to the EC contribution, thus the large K factor will not affect our conclusions. Where the IC and EC components are comparable, the IC K factor is small. Note also that the IC K factor becomes less than unity for $x > 0.2$ depending on $\bar{\nu}$, as can be anticipated from the Fig. 1.

Now let us try to get a good fit to the data with the sum of an EC and an IC component to the structure function. We have performed a least squares fit to the data using the Levenberg-Marquardt algorithm [35]. The normalization of both the IC and EC components are taken as free parameters,

$$F_2^c(x, Q^2, m_c^2) = \alpha \cdot F_2^{c,\mathrm{EC}}(x, Q^2, m_c^2) + \beta \cdot F_2^{c,\mathrm{IC}}(x, Q^2, m_c^2) \ , \qquad (4.1)$$

with the scale $\mu = \mu_0$. The shift in the normalization of the EC component may be considered as an estimate of the size of the NNLO contribution, which is equivalent to a shift in the scale μ. Since we have already assumed a 1% normalization of the IC component, the fitted β is the fraction of this normalization. The results are presented in Table 2. The errors quoted in the table correspond to a 95% confidence level on the central fit parameters. The final results for the combined model of eq. (4.1) are shown in Fig. 7 for the CTEQ3, MRS(G) and GRV94 sets of parton densities. The table shows that given the quality of the data, no statement can be made about the intrinsic charm content for $\bar{\nu} = 53$ and 95 GeV. However, for $\bar{\nu} = 168$ GeV an intrinsic charm contribution of $(0.86 \pm 0.60)\%$ is indicated. For completeness we have examined the influence of a resolving factor, $R(Q^2) = (\mu_s^2 + Q^2)/(4m_c^2 + Q^2)$ where $\mu_s^2 = 0.2\ \mathrm{GeV}^2$ for the IC contribution. This does not alter our conclusions.

We close with some remarks on other recent results. We have already mentioned that another group [10] also checked that recent parton densities

fit the EMC data, using slightly older GRV parton densities [36]. They concentrated on the x and Q^2 regions where there is clearly no IC component in an attempt to use $F_2(x, Q^2, m_c^2)$ for a direct determination of the gluon density in the proton [37]. Therefore there is no overlap with our work. A recent analysis of muon production from IC decays at HERA (and at fixed target facilities) suggests that even an 0.1% IC contribution could be measurable at HERA [38]. We therefore urge experimentalists to make a decisive measurement.

Acknowledgements

The work of B.W. Harris was supported in part under the contracts NSF 93-09888 and DOE-FG05-87ER40319. The work of J. Smith was supported in part under the contract NSF 93-09888. We thank Yu.A. Golubkov for discussions and for providing us with his computer code and J.F. Owens for discussions.

References

[1] J.J. Aubert *et al.*, (EMC), Nucl. Phys. **B 213** (1983) 31; Phys. Lett. **B 94** (1980) 96; ibid. **B110** (1982) 73; M. Strovink, Proceedings of the 1981 International Symposium on Lepton and Photon Interactions at High Energies (Bonn) ed. W. Pfeil, p. 594.

[2] J.C. Collins, D.E. Soper, and G. Sterman in *Perturbative QCD* ed. A.H. Mueller (World Scientific, 1989).

[3] S.J. Brodsky, P. Hoyer, C. Peterson and N. Sakai, Phys. Lett. **B93** (1980) 451; S.J. Brodsky, C. Peterson and N. Sakai, Phys. Rev. **D23** (1981) 2745.

[4] E. Hoffmann and R. Moore, Z. Phys. **C20** (1983) 71.

[5] E. Laenen, S. Riemersma, J. Smith and W.L. van Neerven, Nucl. Phys. **B392** (1993) 162.

[6] S. Riemersma, J. Smith and W.L. van Neerven, Phys. Lett. **B347** (1995) 43.

[7] E. Laenen, S. Riemersma, J. Smith and W.L. van Neerven, Nucl. Phys. **B392** (1993) 229.

[8] B.W. Harris and J. Smith, Nucl. Phys. **B452** (1995) 109.

[9] B.W. Harris and J. Smith, Phys. Lett. **B353** 1995 535.

[10] M. Glück, E. Reya and M. Stratmann, Nucl. Phys. **B422** (1994) 37.

[11] S.J. Brodsky, P. Hoyer, A.H. Mueller, W.-K. Tang, Nucl. Phys. **B369** (1992) 519.

[12] M. Adamovich, *et al.*, WA82 Collaboration, Phys. Lett. **B305** (1993) 402; G.A. Alves *et al.*, E769 Collaboration, Phys. Rev. Lett. **72** (1994) 812; T. Carter, E791 Collaboration, in proceedings of *DPF '94*, the meeting of the APS Division of Particles and Fields, Albuquerque, NM, 1994.

[13] R. Werding, WA89 Collaboration, in proceedings of ICHEP94, Glasgow.

[14] R. Vogt and S.J. Brodsky, Nucl. Phys. **B438**, (1995) 261.

[15] R. Vogt, S.J. Brodsky, and P. Hoyer, Nucl. Phys. **B383** (1992) 643.

[16] T. Sjöstrand, Comput. Phys. Commun. **39** (1986) 347; T. Sjöstrand and M. Bengtsson, Comput. Phys. Commun. **43** (1987) 367; V.G. Kartvelishvili, A.K. Likhoded, and S.R. Slobospitskii, Sov. J. Nucl. Phys. **33**(3) (1981) 434 [Yad. Fiz. **33** (1981) 832]; R.C. Hwa, Phys. Rev. Lett. **51** (1994) 85.

[17] J. Badier *et al.*, Z. Phys. **C20** (1983) 101.

[18] R. Vogt, S.J. Brodsky, and P. Hoyer, Nucl. Phys. **B360** (1991) 67.

[19] J. Badier *et al.*, Phys. Lett. **114B** (1982) 457; Phys. Lett. **158B** (1985) 85.

[20] R. Vogt and S.J. Brodsky, Phys. Lett. **B349** (1995) 569; R. Vogt, LBL-36755 (1995), Nucl. Phys. **B446** (1995) 149.

[21] C. Biino *et. al.*, Phys. Rev. Lett. **58** (1987) 2523; M. Vänttinen, P. Hoyer, S.J. Brodsky, and W.-K. Tang, SLAC-PUB-6637 (1994).

[22] S.J. Brodsky, J.C. Collins, S.D. Ellis, J.F. Gunion, and A.H. Mueller, in *Proceedings of the Summer Study on the Design and Utilization of the Superconducting Super Collider,* Snowmass, CO, 1984, edited by R. Donaldson and J. Morfín (Division of Particles and Fields of the American Physical Society, New York, 1985).

[23] See *e.g.* R.D. Field, Applications of Perturbative QCD, (Addison-Wesley, New York, 1989) p. 358.

[24] Yu.A. Golubkov, DESY preprint, DESY-94-060, April 1994.

[25] R.K. Ellis and P. Nason, Nucl. Phys. **B312** (1989) 551.

[26] S. Frixione, M. L. Mangano, P. Nason and G. Ridolfi, Phys. Lett. **B348** (1995) 633.

[27] J. Smith and W.L. van Neerven, Nucl. Phys. **B374** (1992) 36; W.L. van Neerven, Nucl. Phys. **B29A** (Proc. Suppl.) (1992) 199.

[28] S. Frixione, M.L. Mangano, P. Nason, and G. Ridolfi, Nucl. Phys. **B412** (1994) 225; M.L. Mangano, P. Nason, and G. Ridolfi, Nucl. Phys. **B373** (1992) 295.

[29] H.L. Lai, J. Botts, J. Huston, J.G. Morfín, J.F. Owens, J.W. Qiu, W.K. Tung and H. Weerts, Phys. Rev. **D51** 4763 (1995).

[30] A.D. Martin, R.G. Roberts, and W.J. Stirling, Phys. Lett. **B354** (1995) 155.

[31] M. Glück, E. Reya, and A. Vogt, Z. Phys. **C67** (1995) 433. Ref(32)

[32] For information on the Durham-RAL HEP Database contact M. R. Whalley at m.r.whalley@durham.ac.uk.

[33] F. Halzen and P. Hoyer, Phys. Lett. **154B** (1985) 324.

[34] R.K. Ellis and Z. Kunszt, Nucl. Phys. **B303** (1988) 653.

[35] P.R. Bevington, Data Reduction and Error Analysis for the Physical Sciences, (McGraw-Hill, New York, 1969).

[36] M. Glück, E. Reya, and A. Vogt, Z. Phys. **C52** (1992) 127.

[37] G.A. Schuler, Nucl. Phys. **B299** (1988) 21; A. Ali, G. Ingelman, G.A. Schuler, F. Barreiro, M.A. García, J.F. de Trocóniz, R.A. Eichler and Z. Kunszt, *Heavy quark physics at HERA*, Proc. DESY workshop on HERA physics, DESY, Hamburg (1988), DESY 88-119; A. Ali and D. Wyler in *Physics at HERA*, vol 2 p. 669, Proceedings of the Workshop, DESY, Hamburg, (1991) eds. W. Buchmüller and G. Ingelman; A. Ali, DESY 93-105.

[38] G. Ingelman, L. Jöhnsson and M. Nyberg, Phys. Rev. **D47** (1993) 4872.

Figure Captions

Fig. 1 (a) The IC contributions to the structure function $F_2(x, Q^2, m_c^2)$ at $Q^2 = 7$ GeV: the massless result (2.5) (upper dotted line), the ξ-scaling result (2.6) (dot-dashed line) and the kinematically corrected formula (2.7) (top solid line). Also shown are the NLO corrections given by (2.9), with the leading-log result (2.13) (dashed line), and the full cross result (2.11) (lower dotted line). The sum of (2.7) and (2.9) using (2.11), represents the total IC contribution to $F_2(x, Q^2, m_c^2)$ (lower solid line). (b) Same as part (a) for $Q^2 = 70$ GeV.

Fig. 2 (a) The EC and IC contributions to the proton structure function $F_2(x, Q^2, m_c^2)$ plotted as functions of Q^2 for fixed $\bar{\nu} = 53$ GeV. The curves show the predictions from the EC photon-gluon fusion model (LO: dotted and NLO: solid lines) and from a 1% IC component (LO: dot-dashed and NLO: dashed lines). The data are from the EMC experiment [1] via Durham-RAL HEP data base [32]. (b) The same as (a) for $\bar{\nu} = 95$ GeV. (c) The same as (a) for $\bar{\nu} = 168$ GeV.

Fig. 3 (a) The EMC data for the structure function $F_2(x, Q^2, m_c^2)$ at $\bar{\nu} = 53$ GeV plotted as a function of x together with the EC and IC LO and NLO contributions. The notation for the lines is the same as in Fig. 2. (b) Same as (a) for $\bar{\nu} = 95$ GeV. (c) Same as (a) for $\bar{\nu} = 168$ GeV.

Fig. 4 (a) The EMC data for $F_2(x, Q^2, m_c^2)$ at $\bar{\nu} = 53$ GeV plotted as a function of x together with the EC and IC results. The solid lines are the NLO EC results with $\mu = \mu_0/2$ (upper), $\mu = \mu_0$ (middle), $\mu = 2\mu_0$ (lower). The dotted line is the NLO result for the MRS(G) parton densities with $\mu = \mu_0$, while the dashed line is the result for the GRV94 parton densities with $\mu = \mu_0$. (b) Same as (a) for $\bar{\nu} = 95$ GeV. (c) Same as (a) for $\bar{\nu} = 168$ GeV.

Fig. 5 (a) The K factors for EC production as a function of x for $\bar{\nu} = 53$ GeV. The solid lines are for the CTEQ3 parton densities with $\mu = 2\mu_0$ (upper), $\mu = \mu_0$ (middle) and $\mu = \mu/2$ (lower). The dotted lines is for the MRS(G) parton densities with $\mu = \mu_0$ and the dashed line is for the GRV94 parton densities with $\mu = \mu_0$. (b) The same as (a) for $\bar{\nu} = 95$ GeV. (c) The same as (a) for $\bar{\nu} = 168$ GeV.

		$\langle x \rangle$		
PDF	μ	$\bar{\nu} = 53$ GeV	$\bar{\nu} = 95$ GeV	$\bar{\nu} = 168$ GeV
CTEQ3	$\mu_0/2$	0.12	0.12	0.11
CTEQ3	μ_0	0.12	0.11	0.10
CTEQ3	$2\mu_0$	0.12	0.11	0.10
MRS(G)	μ_0	0.12	0.12	0.11
GRV(94)	μ_0	0.13	0.12	0.11

Table 1:

Fig. 6 The K factors for IC production as a function of x for $\bar{\nu} = 168$ GeV (solid line), $\bar{\nu} = 95$ GeV (dashed line) and $\bar{\nu} = 53$ GeV (dotted line).

Fig. 7 (a) The EMC data for the structure function $F_2(x, Q^2, m_c^2)$ at $\bar{\nu} = 53$ GeV plotted as a function of x together with the fitted results from (4.1). The solid line is for the CTEQ3 parton densities, the dotted line is for the MRS(G) parton densities and the dashed line is for the GRV94 parton densities. The parameters α and β are given in Table 1. (b) Same as (a) for $\bar{\nu} = 95$ GeV. (c) Same as (a) for $\bar{\nu} = 168$ GeV.

Table Caption

Table 1 Average x values of the EC component for $\bar{\nu}$ bins and the various parton densities used in this analysis.

Table 2 Results of the least squares fit of EC and IC contributions to the EMC data according to (4.1). Uncertainties in the fit parameters are shown at the 95% confidence level.

	$\bar{\nu} = 53$ GeV		$\bar{\nu} = 95$ GeV		$\bar{\nu} = 168$ GeV	
PDF	α	β	α	β	α	β
CTEQ3	0.95 ± 0.64	0.36 ± 0.58	1.20 ± 0.13	0.39 ± 0.31	1.27 ± 0.06	0.92 ± 0.53
MRS(G)	1.02 ± 0.69	0.34 ± 0.58	1.38 ± 0.15	0.32 ± 0.32	1.47 ± 0.07	0.79 ± 0.53
GRV(94)	1.15 ± 0.77	0.33 ± 0.58	1.45 ± 0.16	0.34 ± 0.31	1.48 ± 0.08	0.88 ± 0.53

Table 2:

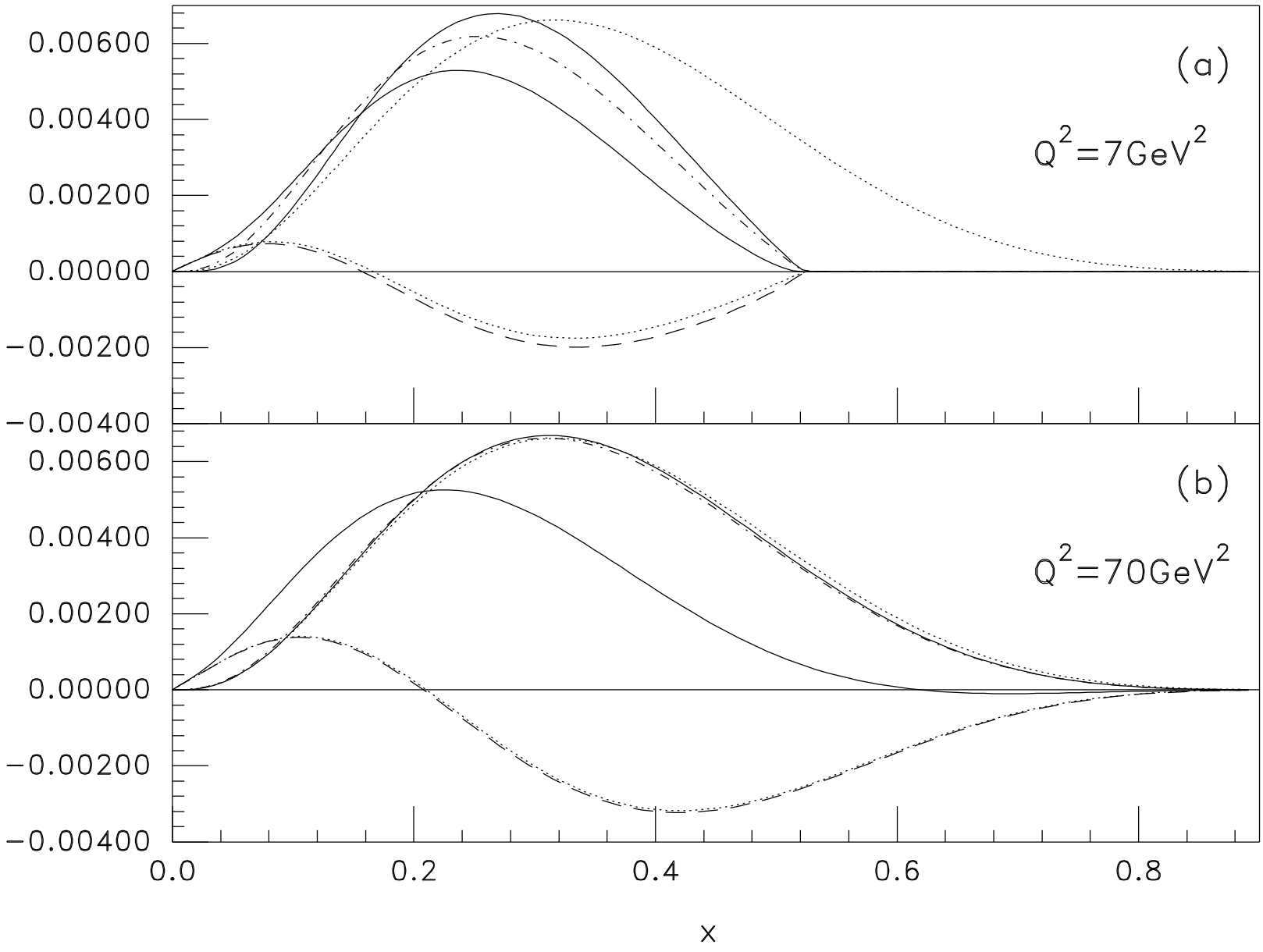
0.00600
0.00400
0.00200
0.00000
−0.00200
−0.00400
(a)
Q^2=7GeV^2
0.00600
0.00400
0.00200
0.00000
−0.00200
−0.00400
(b)
Q^2=70GeV^2
0.0
0.2
0.4
0.6
0.8
x

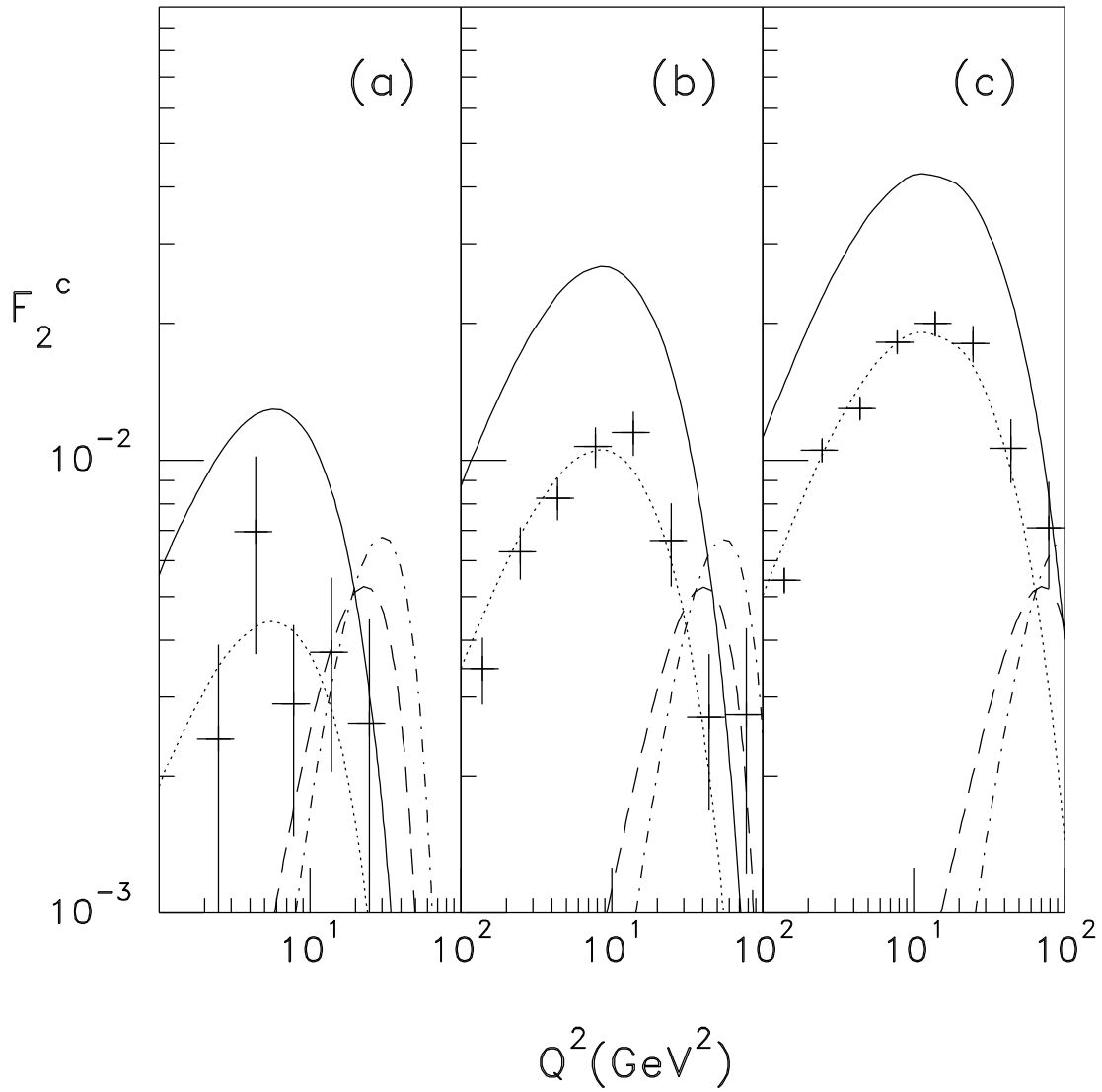
(a)
(b)
(c)
F_2^c
10^{-2}
10^{-3}
10^1
10^2
10^1
10^2
10^1
10^2
$Q^2(GeV^2)$

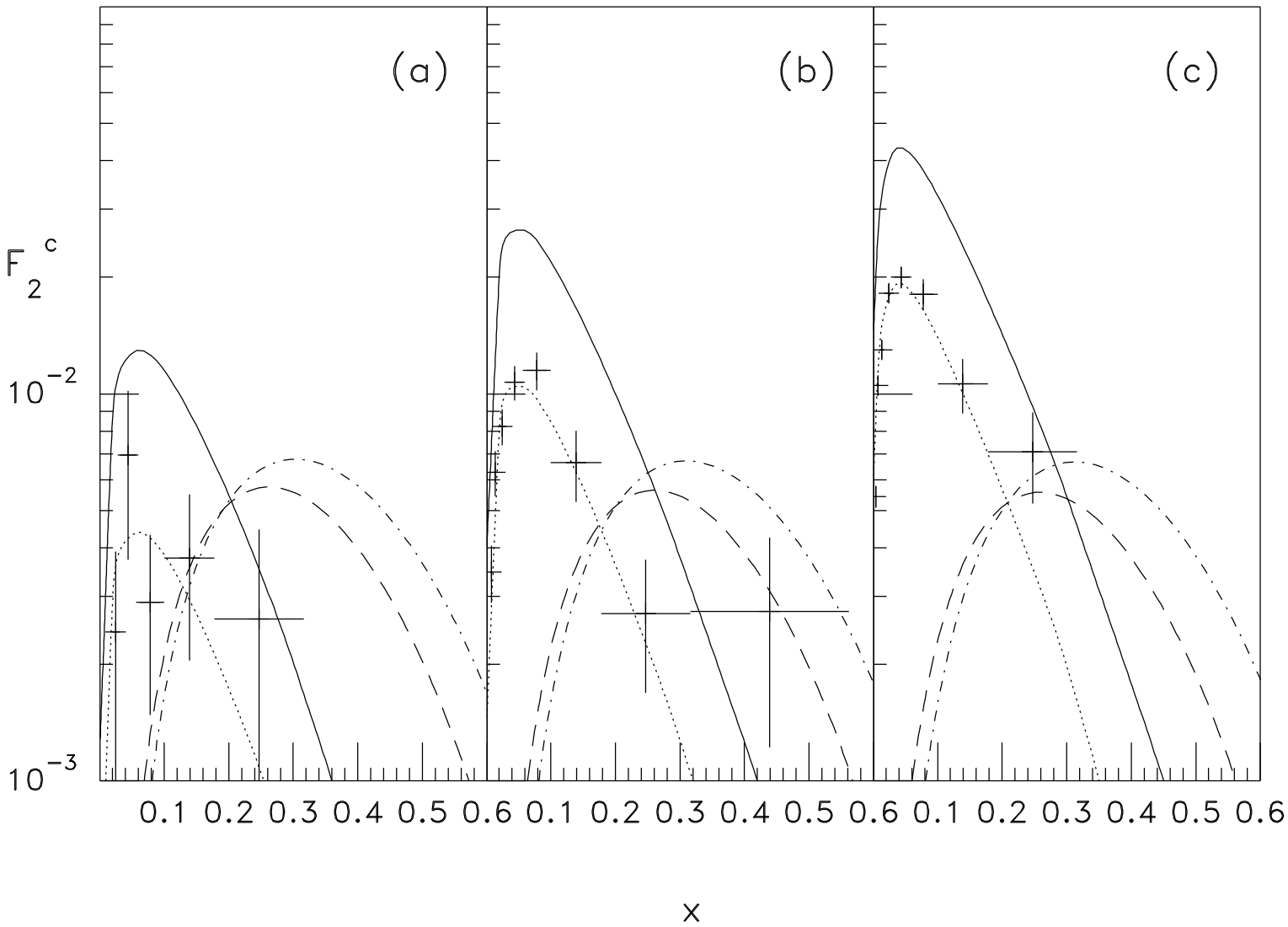
(a)
(b)
(c)
F_2^c
10^{-2}
10^{-3}
0.1 0.2 0.3 0.4 0.5 0.6 0.1 0.2 0.3 0.4 0.5 0.6 0.1 0.2 0.3 0.4 0.5 0.6
x

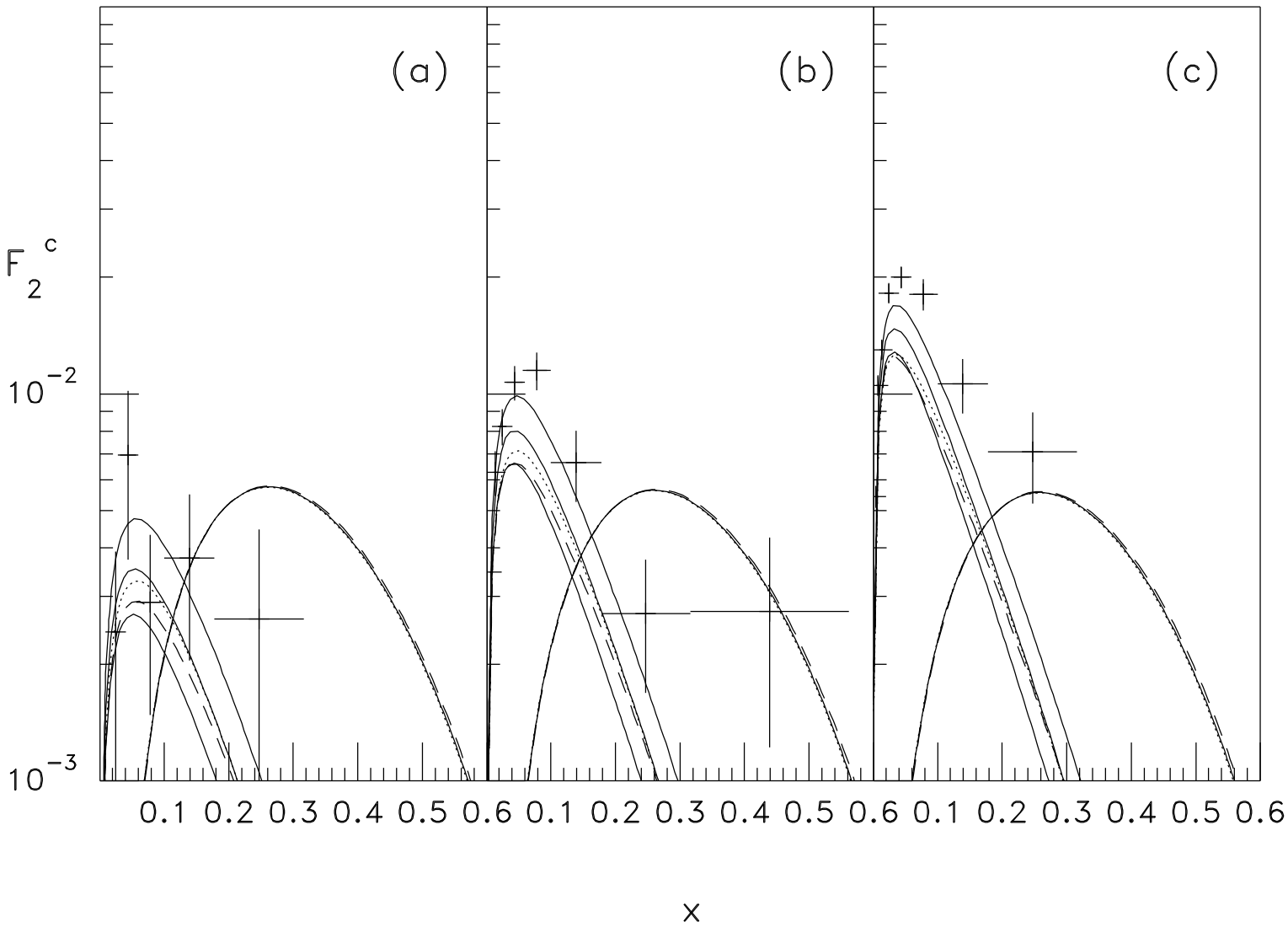
(a)
(b)
(c)
F_2^c
10^{-2}
10^{-3}
0.1 0.2 0.3 0.4 0.5 0.6 0.1 0.2 0.3 0.4 0.5 0.6 0.1 0.2 0.3 0.4 0.5 0.6
x

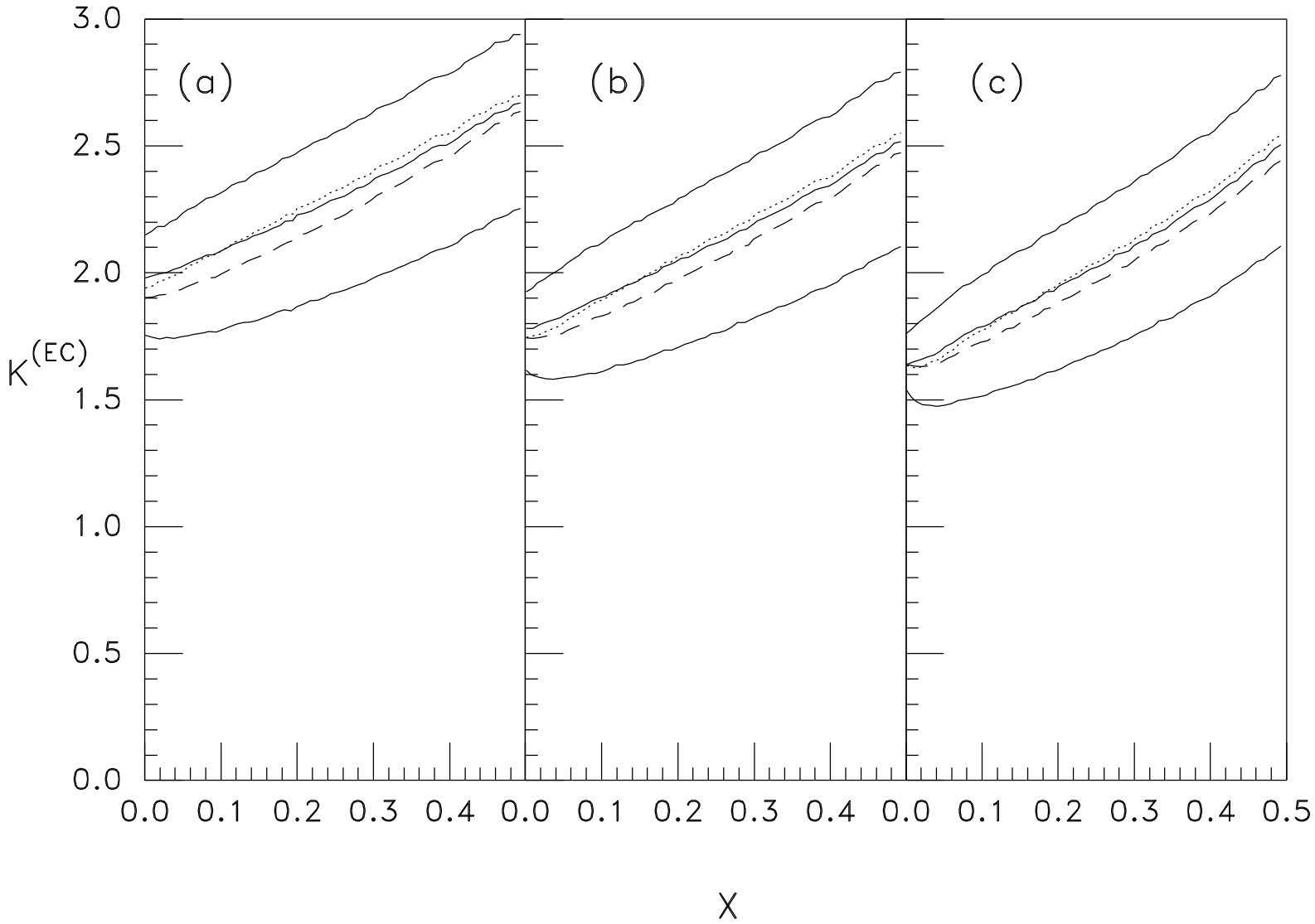
(a)
(b)
(c)
$K^{(EC)}$
3.0
2.5
2.0
1.5
1.0
0.5
0.0
0.0 0.1 0.2 0.3 0.4 0.0 0.1 0.2 0.3 0.4 0.0 0.1 0.2 0.3 0.4 0.5
X

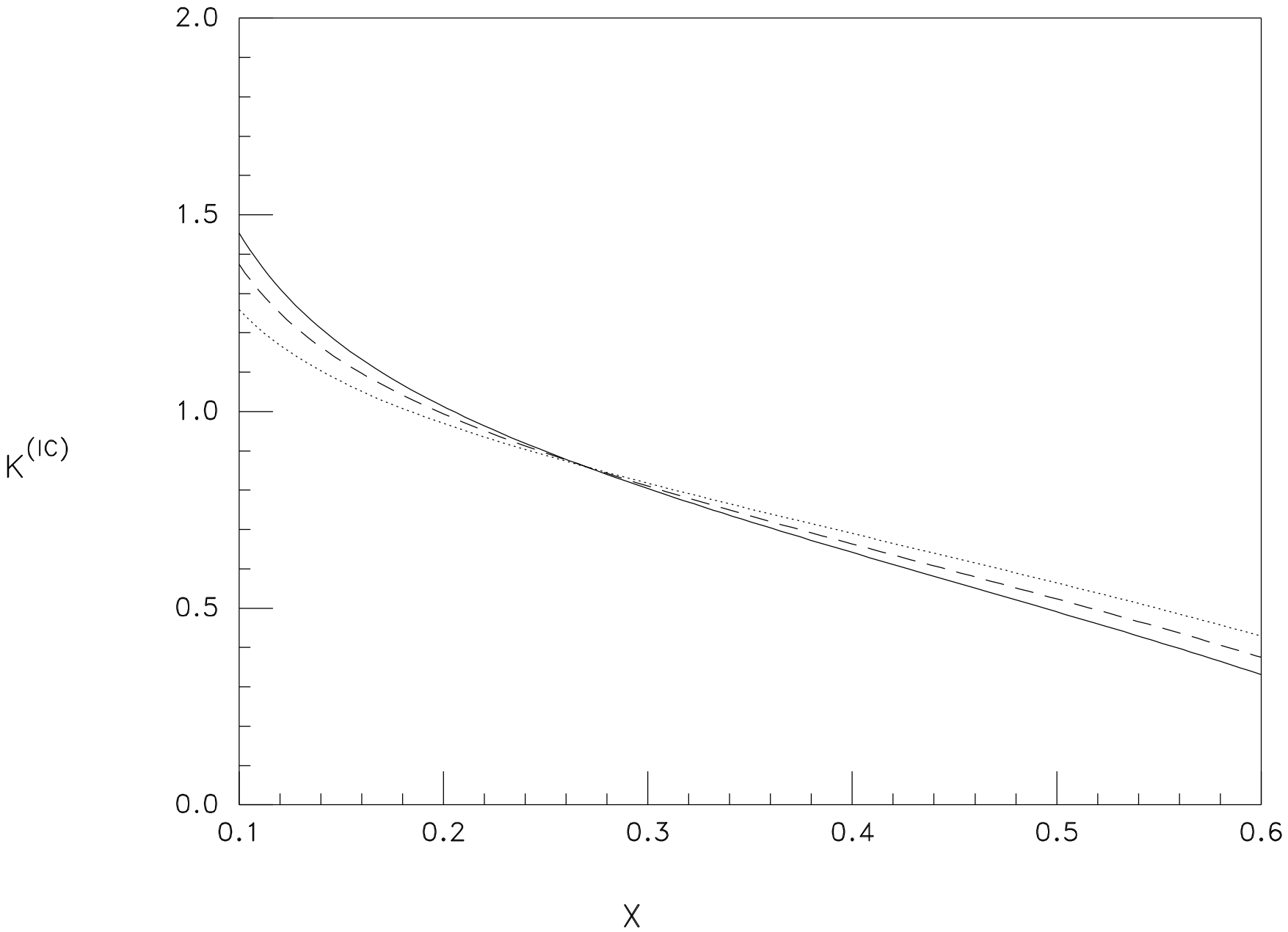
2.0
1.5
1.0
0.5
0.0
0.1
0.2
0.3
0.4
0.5
0.6
K(IC)
X

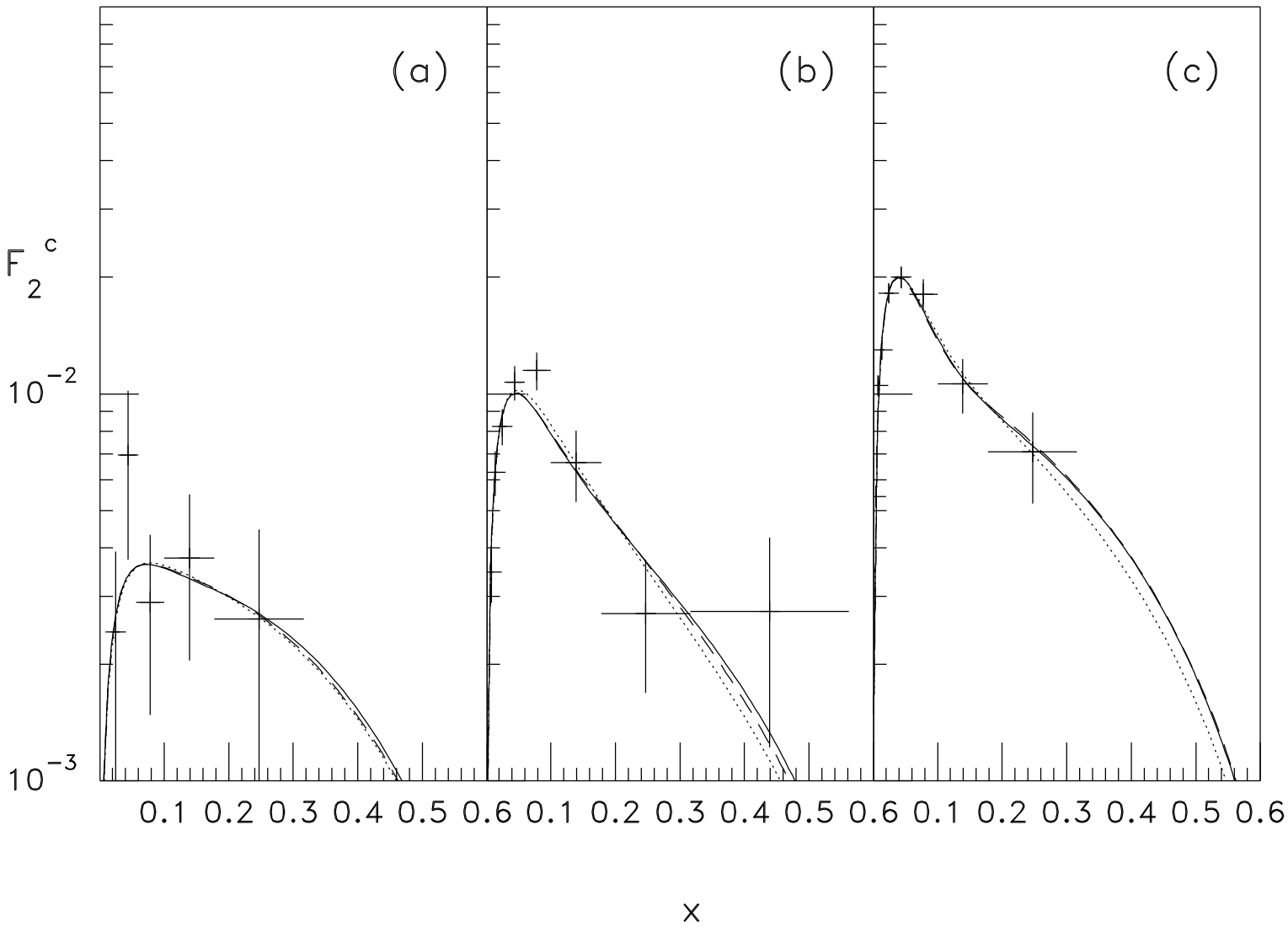
(a)
(b)
(c)
F_2^c
10^{-2}
10^{-3}
0.1 0.2 0.3 0.4 0.5 0.6 0.1 0.2 0.3 0.4 0.5 0.6 0.1 0.2 0.3 0.4 0.5 0.6
x